This paper appears in IEEE Transactions on Control Systems Technology, 2021.
https://doi.org/10.1109/TCST.2021.3107483


# Impedance Learning-based Adaptive Control for Human-Robot Interaction

Mojtaba Sharifi, *Member, IEEE*, Vahid Azimi, *Member, IEEE*, Vivian Mushahwar, *Member, IEEE*, Mahdi Tavakoli, *Senior Member, IEEE,*

***Abstract*—In this paper, a new learning-based time-varying impedance controller is proposed and tested to facilitate an autonomous physical human-robot interaction (pHRI). Novel adaptation laws are formulated for online adjustment of robot impedance based on human behavior. Two other sets of update rules are defined for intelligent coping with the robot's structured and unstructured uncertainties. These rules ensure stability via Lyapunov's theorem and provide uniform ultimate boundedness (UUB) of the closed-loop system's response, without a need for HRI force/torque measurement. Accordingly, the convergence of response signals, including errors in tracking, online impedance learning, robot parameter adaptation, and controller gain variation, is proven to operate in a bounded region (compact set) in the presence of robot and human uncertainties and bounded disturbances. The performance of the developed intelligent impedance-varying control strategy is investigated through comprehensive experimental studies in a repetitive following task with a moving target.**

***Index Terms*—Physical human-robot interaction (pHRI); autonomous impedance variation; nonlinear adaptive control; robot stability; uniformly ultimately boundedness (UUB).**

## I. Introduction

In recent years, the concept of impedance has found an important role in applications involving physical human-robot interactions (pHRI), haptics, and biomedical and industrial robotics. To be effective in such interactions, the robot should comply with the human forces by displaying particular impedance (physical behavior) that needs to be regulated according to the application at hand. Interactive tasks cannot be conducted well by pure position or force controllers [1]. Consequently, the robot impedance regulation has been the focus of many research studies over the past three decades in the fields of robotics and pHRI [2], [3]. Significant research has been conducted to develop sophisticated control strategies for implementing constant impedance while taking the dynamic and kinematic complexities of multi-DOF (degree of freedom) robots into account. Since the pioneering work on impedance and compliance control in the 1980s [4], [5], considerable contributions have been proposed in this area [6]. For instance, robust impedance control [7], [8], hybrid force/motion impedance control [9], and adaptive impedance/admittance control [1], [10] are some classical strategies that have been investigated extensively.

Although the above studies were conducted considering impedance/admittance models with constant parameters, recent investigations have focused on time-varying impedance control and/or online learning of impedance parameters in the joint or Cartesian space of a robot for different applications of pHRI. Enhancing the impedance of robotic systems using these learning and variation strategies has been inspired by the continuous adjustments to the human physical behavior by the central nervous system (CNS) [11], [12], [13], [14], [15], [16]. In this regard, task requirements and human behavior are crucial to modulating the robot impedance parameters autonomously in real-time to improve its task execution performance [17], [18], [19], which requires adequate knowledge about the robot and human modeling.

Systematic time-varying impedance control strategies have been aimed at modulating the stiffness, damping and inertia of the robot in order to improve its interaction with the human/environment while satisfying stability conditions. One of the primary purposes of impedance regulation in pHRI is to maintain velocity and/or force within appropriate ranges [20]. For instance, the precision in performing a pHRI task is provided by subtle movements at low speeds, which can be made possible by imposing high impedance levels. On the other hand, low impedance is required when someone wants to execute large movements at high velocities [14], [21], [22], [23], [24], [25]. To facilitate human manipulation of the robot across these high- and low-velocity scenarios, velocity-dependent varying-impedance control was adopted in [26], [27].

In the same way, the admissible range of damping variation was determined experimentally [21] with the purpose of task execution accuracy and task completion time improvement. The HRI force has been also controlled indirectly [28], [20] by specifying the robot position and adjusting the desired impedance in compliance with the environment boundaries and dynamics. In some procedures such as deburring [29], assembling [30], and surgery [31], it is essential to maintain certain levels of interaction force. Using classical impedance controllers, one can adjust the force indirectly by selecting the robot impedance in accordance with the environmental structure [28]. On the other hand, dynamic and kine-

Manuscript received November 2, 2020; Revised: February 8, 2021; Accepted: July 22, 2021. (*Corresponding author: Mojtaba Sharifi*)

Mojtaba Sharifi and Mahdi Tavakoli are with the Department of Electrical and Computer Engineering, University of Alberta, Edmonton, Alberta, Canada T6G 1H9 (e-mail: M.Sharifi@ualberta.ca; Mahdi.Tavakoli@ualberta.ca).

Mojtaba Sharifi and Vivian Mushahwar are with the Department of Medicine, Division of Physical Medicine and Rehabilitation, University of Alberta, Edmonton, Alberta, Canada T6G 2E1 (e-mail: M.Sharifi@ualberta.ca; Vivian.Mushahwar@ualberta.ca).

Mojtaba Sharifi, Vivian Mushahwar, and Mahdi Tavakoli are with Sensory Motor Adaptive Rehabilitation Technology (SMART) Network, University of Alberta, Edmonton, Alberta, Canada T6G 2E1.

Vahid Azimi is with the Department of Energy Resources Engineering, Stanford University, California, USA (e-mail: Vazimi@stanford.edu).

matic uncertainties of the robot and environment can cause low accuracy in indirect force control. Thereby, force-based variable impedance controllers were proposed in [20], [30], [32] for direct HRI force control considering its continuous differentiability and having sensors for precise force/torque measurement. However, many robotic systems in industrial and medical applications are not equipped with force/torque sensors at all points of their physical interaction [33], [34]. In another work [35], the concept of tele-impedance was investigated for HRI, in which the desired Cartesian end-point stiffness of the robot is adjusted in real-time based on the human arm's stiffness estimated through analyzing the electromyography (EMG) signals of eight muscles acting on the shoulder and elbow joints. A similar impedance-matching strategy was developed in [16] to regulate the joint stiffness of a lower-limb exoskeleton based on the processing of the EMG signals obtained from leg muscles.

Since the variation of impedance parameters may violate stability conditions, it is vital to strike a balance between achieving a desirable performance and stability, especially in applications like medical robotics where human safety is of paramount importance. Therefore, the desired time-varying impedance was modified considering an energy tank as the reservoir of the safe amount of energy that can be utilized without jeopardizing stability [36], [37]. As a result, a trade-off between the stability and time-varying impedance was analytically formulated [36], [37] using the concepts of Lyapunov stability, energy tanks, and passivity conditions [38]. Other passivity-based methods [39], [19] were proposed for robots with flexible joints and/or series elastic actuators (SEAs) having nonlinear stiffness elements, to modify the dynamic response of pHRI without considering any tank-energy levels. Although a direct force measurement is avoided in these studies [19], [36], [37], [39], the modeling uncertainties of HRI were not taken into account.

A state-independent stability condition was obtained by Kronander et al. [40] for changing the stiffness and damping, which was verified offline before task execution. By satisfying certain mathematical constraints in [41], the dynamics of the closed-loop system in the presence of impedance variation was guaranteed to be exponentially stable, and the resulting position, velocity, and acceleration of the robot were bounded in response to interaction forces. In [42], some conditions for varying the impedance parameters were deduced to ensure a stable interaction, where the uncertain robot model was approximated based on a disturbance estimator [43]. While the aforementioned strategies [36], [37], [41], [42] enhanced human safety through improved stability conditions, they suggested deviations from the desired time-varying impedance as a compromise between the robot's performance and its stability. Moreover, they suffered from requiring precise knowledge of robot dynamics parameters and/or having force measurements.

In addition to the methods mentioned above, various impedance learning policies have been proposed for different HRI cases in the past decade [44], [45], [46]. Algorithms of Learning from Demonstration (LfD) have been suggested as a mathematical tool to implement a proper robot behavior via learning based on several initial demonstration steps before the final imitation stage. This has also been extended to pHRI and impedance control recently for learning position trajectories according to the human's movements in the demonstration phase, and then for the regulation of robot impedance in terms of the flexibility around the desired trajectory [47], [48], [49]. Dynamic Movement Primitives (DMPs) [50], [51] as a learning tool for autonomous nonlinear dynamical systems have been utilized to identify the stiffness (or impedance) and the movement of human limbs from EMG signals obtained from typical people for designing the robot impedance controller [52], [53], [54]. Optimizing a cost function in terms of motion variables and interaction forces (in order to explore the optimum robot impedance considering environment/human limb models) has also been adopted in [55], and some optimal controllers have been investigated for the same purpose in [45], [56], [57], [58]. Although these strategies were successful in various robot interactions with dynamically uncertain environments (human limbs), the closed-loop robot stability was not guaranteed in the presence of impedance variations.

To deal with stability issues, model-based impedance adaptation rules have been developed based on the Lyapunov theorem, where the environment (human) behavior was modeled to be non-passive with unknown parameters. Accordingly, some learning-based controllers have enhanced the robot stability in its physical interactions by utilizing appropriate impedance adaptations [59], [44], [60]. Impedance adjustment in response to various high- and low-frequency external forces are beneficial aspects of these strategies that provide a compromise with deviating from the desired trajectory. However, unstructured uncertainties in the robot and human models have not been taken into account and precise knowledge about the dynamic parameters of the robot was assumed.

In the current study, a new impedance-varying control strategy is proposed for autonomous pHRI by which the uniform ultimate boundedness (UUB) of the closed-loop system's response in tracking the desired task trajectory is guaranteed. To this end, an adaptation law is defined for appropriate variation of the robot impedance parameters (stiffness and damping) and an additional feedforward force, based on the online estimation of these properties from the human. Furthermore, two other update rules are defined for the estimation of the robot dynamic parameters and the adjustment of the robot controller's robust gain during the interaction in order to resolve and overcome the structured and unstructured modeling uncertainties of the robot and human, respectively.

By implementing the proposed scheme, with minimal information about the pHRI model and without the use of force measurement, a stable and safe interaction is achieved through the integration of the new adaptation laws. The system's stability and the convergence of tracking error, impedance elements, and controller's gain to their appropriate values are proven using a comprehensive Lyapunov analysis. Accordingly, this control scheme resolves the following issues of previous studies: (i) requiring direct HRI force measurement at the point of interaction [20], [30], [32], (ii) lack of closed-loop stability analysis while providing impedance-varying-based flexibility (trajectory deviation) [35] [45], [47], [48], [49], [52], [53],

[54], [56], [57], [58], and (iii) ignoring modeling uncertainties of HRI dynamics [19], [36], [37], [39], [41], [42]. The possible applications of this autonomous impedance-learning strategy include pHRI tasks for service and medical operations, manufacturing, construction, entertainment and agriculture, where the safety of human users is a great matter of concern, while at the same time, human operators have unknown impedance and force rendering characteristics.

## II. Robot and HRI Dynamic Models

The nonlinear dynamics of a robot manipulator with $n$ joints interacting with the human (environment) is given as

$$M_q(q)\ddot{q}+C_q(q)\dot{q}+G_q(q)+\tau_{fri}(\dot{q})+\tau_{unc}=\tau_{con}+\tau_{hum} \quad (1)$$

where $q$ is the $n\times 1$ vector of robot joint position, $M_q(q)$ is the $n\times n$ inertia matrix, $C_q(q)$ is the $n\times n$ matrix of Coriolis and centrifugal terms, $G_q(q)$ is the $n\times 1$ vector of gravitational torques, $\tau_{fri}$ is the $n\times 1$ vector of the friction torques, $\tau_{unc}$ is the $n\times 1$ vector of unstructured model uncertainties, unmodeled dynamics or disturbances for pHRI (the combination of the robot and the human), $\tau_{con}$ is the $n\times 1$ control torque, and $\tau_{hum}=J^T f_{hum}$ is the $n\times 1$ human torque, $J$ is the $m\times n$ robot Jacobian matrix and $f_{hum}$ is the $m\times 1$ force applied on the robot end-effector by the human. The robot dynamics in the Cartesian space is expressed as [61]

$$M_x(q)\ddot{x}+C_x(q)\dot{x}+G_x(q)+f_{fri}(\dot{q})+f_{unc}=f_{con}+f_{hum} \quad (2)$$

in which $x$ is the $m\times 1$ vector of the robot end-effector position, $M_x=(JM_q^{-1}J^T)^{-1}$ is the $m\times m$ end effector inertia matrix, $C_x=M_x(JM_q^{-1}C_q-\dot{J})J^\dagger$ is the $m\times m$ matrix of the end effector's centrifugal and Coriolis terms, $G_x={J^\dagger}^T G_q$ is the vector of gravitational force and $f_{fri}={J^\dagger}^T\tau_{fri}$ the $m\times 1$ vector of friction force reflected to the end effector, $f_{unc}={J^\dagger}^T\tau_{unc}$ is the $m\times 1$ vector of the unstructured uncertainties and $f_{con}={J^\dagger}^T\tau_{con}$ is the control force transformed to the Cartesian space and generated by joint-space motor torque $\tau_{con}$. Note that the generalized inverse of the Jacobian matrix is defined as $J^\dagger=M_q^{-1}J^T[JM_q^{-1}J^T]^{-1}$.

*Property:* In both joint and Cartesian spaces ($y=q,x$), the robot inertia matrix $M_y$ is positive definite, the matrix $\dot{M}_y-2C_y$ is skew symmetric, and the left side of (1) and (2) can be linearly parameterized [61], [62], [63] as

$$M_y(q)\phi_1+C_y(q)\phi_2+G_y(q)+\tau_{fri}/f_{fri}(\dot{q})=Y_y(\phi_1,\phi_2,q,\dot{q})\theta_y \quad (3)$$

in which $Y_y$ is the regressor matrix defined in terms of known variables including $\phi_1$ and $\phi_2$, and $\theta_y$ is the vector of unknown parameters of the robot dynamics. As proven and presented in [44], [60], the following three-term model is considered for the human-robot interaction force:

$$f_{hum}(t)=f_{ff}(t)+K_h(t)e_x(t)+B_h(t)\dot{e_x}(t) \quad (4)$$

where $f_{ff}$ is the feedforward force of the human, and the second and third terms are the stiffness-based and damping-based elements of the human force in physical interactions when they deviate from the desired robot trajectory. The Cartesian position and velocity errors are defined as $e_x(t)=x(t)-x_{des}(t)$ and $\dot{e_x}(t)=\dot{x}(t)-\dot{x}_{des}(t)$ where $x_{des}(t)$ is the desired robot trajectory in any pHRI task. Note that the unstructured uncertainties (modeling mismatch) for both of the robot and human is denoted by $f_{unc}$ in Eq. (2), which is bounded:

$$|f_{unc}|\leq\eta_x \quad (5)$$

where $|.|$ gives the element-wise absolute vector. $\eta_x$ is an unknown positive vector with elements greater than or equal to the upper bounds of $|f_{unc}|$ elements. As these upper bounds can vary during the operation, $\eta_x$ needs to be estimated and/or compensated over time (e.g., by adjusting the robust controller gains).

As mentioned earlier, one of the main issues of HRI is adapting the physical behavior of the robot to human interaction while tracking the predefined trajectory of a task. This becomes more challenging when we have uncertainties in HRI modeling in the absence of force/torque sensors at the point of interaction, which is the case in different applications such as industrial robotics, assistive devices, and exoskeletons. This problem is tackled in this research work by enhancing the robot autonomy via estimating the human force and learning the impedance components of the physical human interaction while preserving the robot's stability. The performance of this intelligent control scheme is assessed with respect to the bounds of human force estimation, impedance adaptation convergence, and trajectory deviation.

## III. Adaptive Impedance-Learning Controller Design

The objective of this autonomous control strategy is to provide a stable pHRI having the combined dynamics (2) and (4) with modeling uncertainties. For this purpose, the control force $f_{con}$ in (2) is designed to achieve bounded tracking of desired task trajectory while adapting the robot impedance in real-time based on human behavior without any force measurement.

### A. Integrated Control Laws

The proposed controller is designed as a combination of three schemes to deal with human impedance, robot dynamics nonlinearities and pHRI uncertainties:

$$f_{con}=f_{con_{non}}+f_{con_{imp}}+f_{con_{sli}} \quad (6)$$

in which $f_{con_{non}}$ stands for the nonlinear terms of the controller employed to compensate for the nonlinear robot dynamics:

$$f_{con_{non}}=\hat{M}_x\ddot{x}_{ref}+\hat{C}_x\dot{x}_{ref}+\hat{G}_x+\hat{f}_{fri}-\sigma\hat{M}_x \quad (7)$$

where $\sigma$ is a constant gain, and the accent $\hat{}$ implies the estimated values of matrices and vectors obtained from an appropriate update rule. The reference velocity $\dot{x}_{ref}$ and the tracking error surface $\epsilon_x$ are defined in terms of the desired trajectory $x_{des}(t)$ and the tracking error $e_x(t)$ as

$$\begin{aligned}\dot{x}_{ref}&=\dot{x}_{des}-\zeta(x-x_{des})=\dot{x}_{des}-\zeta e_x\\ \epsilon_x&=\dot{e}_x+\zeta e_x\end{aligned} \quad (8)$$

such that $\epsilon_x = \dot{x} - \dot{x}_{ref}$ and $\zeta$ is the constant factor scaling between position and velocity errors. The control input (7) can be reformulated regarding the property (3) as

$$f_{con_{non}} = Y_x(\ddot{x}_{ref} - \sigma\epsilon_x, \dot{x}_{ref}, q, \dot{q})\hat{\theta}_x(t) \tag{9}$$

The control scheme $f_{con_{imp}}$ is designed to adjust the robot impedance online in order to compensate for the HRI force based on the model (4):

$$f_{con_{imp}} = -\hat{f}_{ff}(t) - \hat{K}_h(t)e_x - \hat{B}_h(t)\dot{e}_x \tag{10}$$

where the accent $\hat{}$ indicates the learned values of feedforward and feedback terms of the human force determined from suitable adaptation laws. The last part of the control law (6) is formulated to overcome unstructured uncertainties and/or unknown disturbances using a robust sliding-mode control (SMC) scheme as

$$f_{con_{sli}} = -\hat{\eta}_x(t) \circ \tanh(\epsilon_x/\beta) \tag{11}$$

where $\hat{\eta}_x$ is the time-varying gain of this robust term updated with an additional adaptation law. $\tanh(\epsilon_x/\beta)$ is the element-wise hyperbolic tangent function of the vector $\epsilon_x/\beta$ and "$\circ$" denotes the Hadamard (element-wise) product. $\beta$ adjusts the slope of this function around $\epsilon_x = 0$, where decreasing its value drives the function steeper in the vicinity of origin ($\epsilon_x = 0$) and closer to the discontinuous sign function $\text{sgn}(\epsilon_x)$. There is a trade-off between increasing $\beta$ for making less variation in the control effort during the convergence to the surface of $\epsilon_x = 0$ and reducing this constant to enhance the effectiveness of this robust term for overcoming uncertainties and achieving smaller tracking errors.

### B. Closed-Loop pHRI Dynamics

The control laws (6)-(11) are substituted in the robot dynamics (2) in order to obtain the closed-loop dynamics of the proposed pHRI system:

$$\begin{aligned} M_x(\ddot{x} - \ddot{x}_{ref}) + C_x(\dot{x} - \dot{x}_{ref}) = \\ - \sigma M_x\epsilon_x + (\hat{M}_x - M_x)(\ddot{x}_{ref} - \sigma\epsilon_x) \\ + (\hat{C}_x - C_x)\dot{x}_{ref} + (\hat{G}_x - G_x) + (\hat{f}_{fri} - f_{fri}) \\ - (\hat{f}_{ff} - f_{ff}) - (\hat{K}_h - K_h)e_x - (\hat{B}_h - B_h)\dot{e_x} \\ - \hat{\eta}_x \circ \tanh(\epsilon_x/\beta) + f_{unc} \end{aligned} \tag{12}$$

Due to the definitions in (8) and after some simplifications in presenting the estimation errors in matrices and vectors, Eq. (12) is rewritten as

$$\begin{aligned} M_x\dot{\epsilon}_x + C_x\epsilon_x = \\ - \sigma M_x\epsilon_x + \tilde{M}_x(\ddot{x}_{ref} - \sigma\epsilon_x) + \tilde{C}_x\dot{x}_{ref} + \tilde{G}_x + \tilde{f}_{fri} \\ - \tilde{f}_{ff} - \tilde{K}_he_x - \tilde{B}_h\dot{e_x} - \hat{\eta}_x \circ \tanh(\epsilon_x/\beta) + f_{unc} \end{aligned} \tag{13}$$

where the accent $\tilde{}$ denotes the estimation error. Based on the robot dynamics property (3), the closed-loop dynamics is obtained as

$$\begin{aligned} M_x\dot{\epsilon}_x + C_x\epsilon_x = - \sigma M_x\epsilon_x + Y_x(\ddot{x}_{ref} - \sigma\epsilon_x, \dot{x}_{ref}, q, \dot{q})\tilde{\theta}_x \\ -\tilde{f}_{ff} - \tilde{K}_he_x - \tilde{B}_h\dot{e_x} - \hat{\eta}_x \circ \tanh(\epsilon_x/\beta) + f_{unc}. \end{aligned} \tag{14}$$

### C. Adaptation/Learning Laws

In this section, different update rules for estimating the robot parameters, learning the robot impedance, and updating its control gains (based on the physical human behavior) in Section III-A are defined. By implementing these rules in the control laws (6)-(11), with minimal information about the pHRI model and without the use of force measurement, a stable and safe interaction is achieved. This is facilitated by tracking the desired task trajectory in terms of the UUB of the closed-loop system's response. For this purpose, an adaptation law is defined for appropriate variation of the robot impedance parameters (stiffness and damping) and an additional feedforward force based on the online estimation of these properties from the human. Two other update rules are defined for the estimation of the robot dynamic parameters and the adjustment of the robust gain of the robot controller during the interaction. These rules augment the intelligent controller to resolve and overcome the structured and unstructured uncertainties of the robot and human models.

The following adaptation law is firstly presented to update the estimation of dynamic parameters $\hat{\theta}_x$ in (9) in terms of the error dynamics and the regressor matrix:

$$\dot{\hat{\theta}}_x(t) = -\Lambda_\theta Y_x^T(\ddot{x}_{ref} - \sigma\epsilon_x, \dot{x}_{ref}, q, \dot{q})\epsilon_x - \Psi_\theta \left\|\epsilon_x\right\| \hat{\theta}_x(t) \tag{15}$$

in which $\Lambda_\theta$ and $\Psi_\theta$ are positive definite matrices as the adaptation gains, and $\|.\|$ denotes the second norm for any vector in this paper. The second adaptation law is designed to learn the human impedance parameters and feedforward force appropriately to adjust them for the robot based on (10) with a small bounded difference as analyzed in the stability proof (described in the next section):

$$\begin{aligned} \dot{\hat{K}}_h(t) &= \Lambda_K\epsilon_x e_x^T - \Psi_K \left\|\epsilon_x\right\| \hat{K}_h(t) \\ \dot{\hat{B}}_h(t) &= \Lambda_B\epsilon_x \dot{e}_x^T - \Psi_B \left\|\epsilon_x\right\| \hat{B}_h(t) \\ \dot{\hat{f}}_{ff}(t) &= \Lambda_f\epsilon_x - \Psi_f \left\|\epsilon_x\right\| \hat{f}_{ff}(t) \end{aligned} \tag{16}$$

where $\Lambda_K$, $\Lambda_B$, $\Lambda_f$, $\Psi_K$, $\Psi_B$ and $\Psi_f$ are positive definite matrices employed as the learning rates of the pHRI impedance. The third update rule is proposed for the sliding-mode gain $\eta_x$ of the controller's robust term (11), which was defined to be the upper bounds of $|f_{unc}|$ in (5)

$$\dot{\hat{\eta}}_x(t) = \Lambda_\eta|\epsilon_x| - \Psi_\eta \left\|\epsilon_x\right\| \hat{\eta}_x(t) \tag{17}$$

in which $\Lambda_\eta$ and $\Psi_\eta$ are positive definite matrices as the update rates. Note that the gains $\Lambda_i$ and $\Psi_i$ in any of the above adaptation laws (15), (16) and (17) imply a compromise between tracking convergence and stability/flexibility of the controlled pHRI. In other words, $\Lambda_i$ represents the weight of trajectory tracking error in comparison with $\Psi_i$ that corresponds to the authority of robot to have physical flexibility and its permission to deviate from the desired trajectory to ensure the stability (investigated in the next section). The terms include $\Psi_i$ in the above-mentioned update rules result in reduction of the adaptive dynamic parameters, impedance elements and SMC gain, as the norm of error ($||\epsilon_x||$) increases, which relax more the control laws (7), (10) and (11).

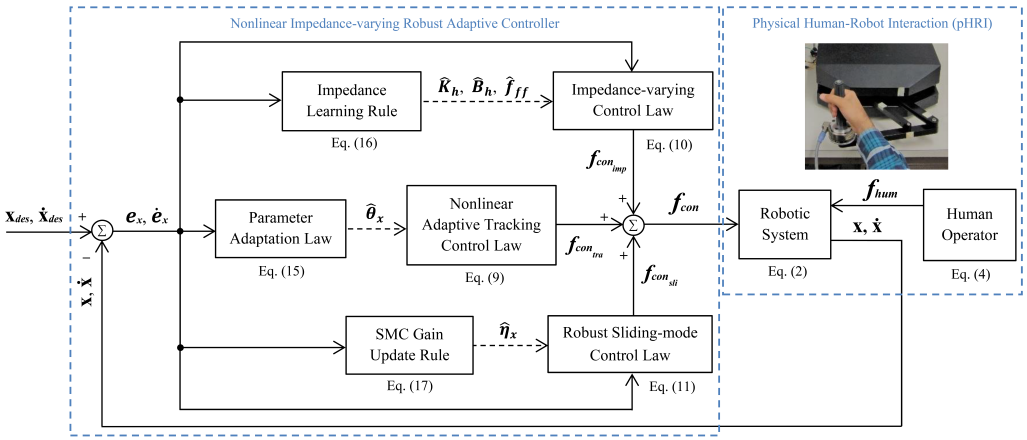


Fig. 1. Schematics of the proposed Lyapunov-based adaptive impedance-learning control strategy

A schematic diagram of this Lyapunov-based impedance-learning controller is shown in Fig. 1. As described in this section, the proposed impedance control and adaptation laws in this learning-based strategy are defined without using any force measurements. In the next section, we prove that these control and adaptation laws (7), (10), (11), (15), (16) and (17) achieve Lyapunov stability of the controlled pHRI by appropriately handling structured robot uncertainties, estimating unknown human impedance and overcoming unknown modeling mismatches (or disturbances).

## IV. Lyapunov Stability Analysis

The following Lyapunov function is defined in order to analyze the stability of the nonlinear closed-loop robot dynamics and the uniform ultimate boundedness (UUB) of the system response:

$$
\begin{aligned}
V(t) &= V_p(t) + V_i(t) + V_s(t) + V_u(t) \\
V_p(t) &= \frac{1}{2}\epsilon_x^T M_x \epsilon_x \\
V_i(t) &= \frac{1}{2}\tilde{f}_{ff}^T \Lambda_f^{-T} \tilde{f}_{ff} \\
&\quad + \frac{1}{2} tr(\tilde{K}_h^T \Lambda_K^{-T} \tilde{K}_h) + \frac{1}{2} tr(\tilde{B}_h^T \Lambda_B^{-T} \tilde{B}_h) \\
V_s(t) &= \frac{1}{2}\tilde{\theta}_x^T \Lambda_\theta^{-T} \tilde{\theta}_x \\
V_u(t) &= \frac{1}{2}\tilde{\eta}_x^T \Lambda_\eta^{-T} \tilde{\eta}_x
\end{aligned}
\tag{18}
$$

in which the superscript $\tilde{}$ is the estimation/adaptation error sign ($\tilde{r} = \hat{r} - r$ for any vector/matrix $r$), and $tr$ stands for the trace of matrices. $\Lambda$, $\Lambda_K$, $\Lambda_B$, $\Lambda_\theta$ and $\Lambda_\eta$ are positive-definite constant matrices as the adaptation gains for the robot impedance and dynamics, and the controller gain employed in Section III-C. The functions $V_p$, $V_i$, $V_s$ and $V_u$ are defined in terms of position, human impedance estimation, robot parameter estimation errors (structured uncertainty) and the robust gain difference with respect to the bound of unstructured uncertainties, whose time derivatives are determined as

$$
\begin{aligned}
\dot{V}_p(t) &= \epsilon_x^T M_x \dot{\epsilon}_x + \frac{1}{2}\epsilon_x^T \dot{M}_x \epsilon_x \\
\dot{V}_i(t) &= (\dot{\hat{f}}_{ff} - \dot{f}_{ff})^T \Lambda_f^{-T} \tilde{f}_{ff} \\
&\quad + tr((\dot{\hat{K}}_h^T - \dot{K}_h^T)\Lambda_K^{-T}\tilde{K}_h) \\
&\quad + tr((\dot{\hat{B}}_h^T - \dot{B}_h^T)\Lambda_B^{-T}\tilde{B}_h) \\
\dot{V}_s(t) &= \dot{\hat{\theta}}_x^T \Lambda_\theta^{-T} \tilde{\theta}_x \\
\dot{V}_u(t) &= (\dot{\hat{\eta}}_x^T - \dot{\eta}_x^T)\Lambda_\eta^{-T}\tilde{\eta}_x
\end{aligned}
\tag{19}
$$

Substituting $M_x \dot{\epsilon}_x$ from the closed-loop dynamics (14), the robot parameter adaptation law (15), the impedance adaptation rule (16) and the SMC gain update rule (17) into Eq. (19) yields

$$
\begin{aligned}
\dot{V}_p(t) =& -\sigma \epsilon_x^T M_x \epsilon_x \\
&- \epsilon_x^T \tilde{f}_{ff} - \epsilon_x^T \tilde{K}_h e_x - \epsilon_x^T \tilde{B}_h \dot{e_x} \\
&+ \epsilon_x^T Y_x \tilde{\theta}_x - \epsilon_x^T \hat{\eta}_x \circ \tanh(\epsilon_x/\beta) + \epsilon_x^T f_{unc} \\
&- \epsilon_x^T C_x \epsilon_x + \frac{1}{2}\epsilon_x^T \dot{M}_x \epsilon_x \\
\dot{V}_i(t) =& \epsilon_x^T \tilde{f}_{ff} - \|\epsilon_x\| \hat{f}_{ff}^T \Psi_f^T \Lambda_f^{-T} \tilde{f}_{ff} - \dot{f}_{ff}^T \Lambda_f^{-T} \tilde{f}_{ff} \\
&+ tr(e_x \epsilon_x^T \tilde{K}_h - \|\epsilon_x\| \hat{K}_h^T \Psi_K^T \Lambda_K^{-T} \tilde{K}_h - \dot{K}_h^T \Lambda_K^{-T} \tilde{K}_h) \\
&+ tr(\dot{e}_x \epsilon_x^T \tilde{B}_h - \|\epsilon_x\| \hat{B}_h^T \Psi_B^T \Lambda_B^{-T} \tilde{B}_h - \dot{B}_h^T \Lambda_B^{-T} \tilde{B}_h) \\
\dot{V}_s(t) =& -\epsilon_x^T Y_x \tilde{\theta}_x - \|\epsilon_x\| \hat{\theta}_x^T \Psi_\theta^T \Lambda_\theta^{-T} \tilde{\theta}_x \\
\dot{V}_u(t) =& |\epsilon_x|^T \tilde{\eta}_x - \|\epsilon_x\| \hat{\eta}_x^T \Psi_\eta^T \Lambda_\eta^{-T} \tilde{\eta}_x - \dot{\eta}_x^T \Lambda_\eta^{-T} \tilde{\eta}_x
\end{aligned}
\tag{20}
$$

***Lemma.*** Given a positive constant $\beta$, the following inequality is valid for each element of $\epsilon_x(i) \in \mathbb{R}$ [64]:

$$
0 \leq |\epsilon_x(i)| - \epsilon_x(i)\tanh(\epsilon_x(i)/\beta) \leq c\,\beta \tag{21}
$$

where $c = 0.2785$.

Due the skew symmetricity of $\dot{M}_x - 2C_x$ as the robot dynamics property, and based on the above *Lemma* and the

fact that $tr(AB) = tr(BA)$ when $A$ and $B$ are $m \times n$ and $n \times m$ matrices, one can write:

$$\begin{aligned}
\dot{V}_p(t) \leq & -\sigma\epsilon_x^T M_x \epsilon_x \\
& - \epsilon_x^T \tilde{f}_{ff} - \epsilon_x^T \tilde{K}_h e_x - \epsilon_x^T \tilde{B}_h \dot{e}_x \\
& + \epsilon_x^T Y_x \tilde{\theta}_x - |\epsilon_x|^T \hat{\eta}_x + [c\beta]_{n\times 1}^T \hat{\eta}_x + \epsilon_x^T f_{unc} \\
\dot{V}_i(t) = & \epsilon_x^T \tilde{f}_{ff} - \|\epsilon_x\| \hat{f}_{ff}^T \Psi_f^T \Lambda_f^{-T} \tilde{f}_{ff} - \dot{f}_{ff}^T \Lambda_f^{-T} \tilde{f}_{ff} \\
& + \epsilon_x^T \tilde{K}_h e_x - tr(\|\epsilon_x\| \hat{K}_h^T \Psi_K^T \Lambda_K^{-T} \tilde{K}_h + \dot{K}_h^T \Lambda_K^{-T} \tilde{K}_h) \\
& + \epsilon_x^T \tilde{B}_h \dot{e}_x - tr(\|\epsilon_x\| \hat{B}_h^T \Psi_B^T \Lambda_B^{-T} \tilde{B}_h + \dot{B}_h^T \Lambda_B^{-T} \tilde{B}_h) \\
\dot{V}_s(t) = & -\epsilon_x^T Y_x \tilde{\theta}_x - \|\epsilon_x\| \hat{\theta}_x^T \Psi_\theta^T \Lambda_\theta^{-T} \tilde{\theta}_x \\
\dot{V}_u(t) = & |\epsilon_x|^T (\hat{\eta}_x - \eta_x) - \|\epsilon_x\| \hat{\eta}_x^T \Psi_\eta^T \Lambda_\eta^{-T} \tilde{\eta}_x - \dot{\eta}_x^T \Lambda_\eta^{-T} \tilde{\eta}_x
\end{aligned} \tag{22}$$

in which all elements of the vector $[c\beta]_{n\times 1}$ equal $c\beta$ defined in (21). Conducting some simplifications and subtracting some terms in $\dot{V}_p$ by others in $\dot{V}_i$, $\dot{V}_s$ and $\dot{V}_u$, the time derivative of the Lyapunov function (18) is obtained as

$$\begin{aligned}
\dot{V}(t) \leq & -\sigma\epsilon_x^T M_x \epsilon_x + \epsilon_x^T f_{unc} - |\epsilon_x|^T \eta_x + [c\beta]_{n\times 1}^T \hat{\eta}_x \\
& - \|\epsilon_x\| \hat{f}_{ff}^T \Psi_f^T \Lambda_f^{-T} \tilde{f}_{ff} - \dot{f}_{ff}^T \Lambda_f^{-T} \tilde{f}_{ff} \\
& - tr(\|\epsilon_x\| \hat{K}_h^T \Psi_K^T \Lambda_K^{-T} \tilde{K}_h + \dot{K}_h^T \Lambda_K^{-T} \tilde{K}_h) \\
& - tr(\|\epsilon_x\| \hat{B}_h^T \Psi_B^T \Lambda_B^{-T} \tilde{B}_h + \dot{B}_h^T \Lambda_B^{-T} \tilde{B}_h) \\
& - \|\epsilon_x\| \hat{\theta}_x^T \Psi_\theta^T \Lambda_\theta^{-T} \tilde{\theta}_x \\
& - \|\epsilon_x\| \hat{\eta}_x^T \Psi_\eta^T \Lambda_\eta^{-T} \tilde{\eta}_x - \dot{\eta}_x^T \Lambda_\eta^{-T} \tilde{\eta}_x
\end{aligned} \tag{23}$$

As seen, the proposed adaptation laws substituted into $\dot{V}(t)$ can compensate for the human impedance estimation errors ($\tilde{K}_h$, $\tilde{B}_h$ and $\tilde{f}_{ff}$) and overcome the structured and unstructured uncertainties ($\tilde{\theta}_x$ and $f_{unc}$). Taking the inequality (5) into account and substituting $\hat{r} = \tilde{r} + r$ for any estimated vector/matrix $r$ into Eq. (23) result in:

$$\begin{aligned}
\dot{V}(t) \leq & -\sigma\epsilon_x^T M_x \epsilon_x + [c\beta]_{n\times 1}^T \tilde{\eta}_x + [c\beta]_{n\times 1}^T \eta_x \\
& - \|\epsilon_x\| \tilde{f}_{ff}^T \Psi_f^T \Lambda_f^{-T} \tilde{f}_{ff} - \|\epsilon_x\| f_{ff}^T \Psi_f^T \Lambda_f^{-T} \tilde{f}_{ff} - \dot{f}_{ff}^T \Lambda_f^{-T} \tilde{f}_{ff} \\
& - tr(\|\epsilon_x\| \tilde{K}_h^T \Psi_K^T \Lambda_K^{-T} \tilde{K}_h + \|\epsilon_x\| K_h^T \Psi_K^T \Lambda_K^{-T} \tilde{K}_h + \dot{K}_h^T \Lambda_K^{-T} \tilde{K}_h) \\
& - tr(\|\epsilon_x\| \tilde{B}_h^T \Psi_B^T \Lambda_B^{-T} \tilde{B}_h + \|\epsilon_x\| B_h^T \Psi_B^T \Lambda_B^{-T} \tilde{B}_h + \dot{B}_h^T \Lambda_B^{-T} \tilde{B}_h) \\
& - \|\epsilon_x\| \tilde{\theta}_x^T \Psi_\theta^T \Lambda_\theta^{-T} \tilde{\theta}_x - \|\epsilon_x\| \theta_x^T \Psi_\theta^T \Lambda_\theta^{-T} \tilde{\theta}_x \\
& - \|\epsilon_x\| \tilde{\eta}_x^T \Psi_\eta^T \Lambda_\eta^{-T} \tilde{\eta}_x - \|\epsilon_x\| \eta_x^T \Psi_\eta^T \Lambda_\eta^{-T} \tilde{\eta}_x - \dot{\eta}_x^T \Lambda_\eta^{-T} \tilde{\eta}_x
\end{aligned} \tag{24}$$

Based on the positive definiteness of $M_x$, $\Lambda_i$ and $\Psi_i$ (for $i = f, K, B, \theta, \eta$), one can write:

$$\begin{aligned}
\dot{V}(t) \leq & \underbrace{-\sigma Q_M \|\epsilon_x\|^2}_{A_\epsilon} + \underbrace{[c\beta]_{n\times 1}^T \eta_x}_{A_0} \\
& \underbrace{-Q_f \|\epsilon_x\| \left\|\tilde{f}_{ff}\right\|^2 + Q_{f_1} \|\epsilon_x\| \left\|\tilde{f}_{ff}\right\| + Q_{f_2} \left\|\tilde{f}_{ff}\right\|}_{A_f} \\
& \underbrace{-Q_K \|\epsilon_x\| \left\|\tilde{K}_h\right\|^2 + Q_{K_1} \|\epsilon_x\| \left\|\tilde{K}_h\right\| + Q_{K_2} \left\|\tilde{K}_h\right\|}_{A_K} \\
& \underbrace{-Q_B \|\epsilon_x\| \left\|\tilde{B}_h\right\|^2 + Q_{B_1} \|\epsilon_x\| \left\|\tilde{B}_h\right\| + Q_{B_2} \left\|\tilde{B}_h\right\|}_{A_B} \\
& \underbrace{-Q_\theta \|\epsilon_x\| \left\|\tilde{\theta}_x\right\|^2 + Q_{\theta_1} \|\epsilon_x\| \left\|\tilde{\theta}_x\right\|}_{A_\theta} \\
& \underbrace{-Q_\eta \|\epsilon_x\| \|\tilde{\eta}_x\|^2 + Q_{\eta_1} \|\epsilon_x\| \|\tilde{\eta}_x\| + Q_{\eta_2} \|\tilde{\eta}_x\|}_{A_\eta}
\end{aligned} \tag{25}$$

where the following non-negative norms ($Q_i$) of matrices and vectors are employed: $Q_M = \lambda_{min}(M_x)$, $\lambda_{min}(\Psi_f^T \Lambda_f^{-T}) = Q_f$, $||f_{ff}^T \Psi_f^T \Lambda_f^{-T}|| \leq Q_{f_1}$, $||\dot{f}_{ff}^T \Lambda_f^{-T}|| \leq Q_{f_2}$, $Q_K = \lambda_{min}(\Psi_K^T \Lambda_K^{-T})$, $||K_h^T \Psi_K^T \Lambda_K^{-T}|| \leq Q_{K_1}$, $||\dot{K}_h^T \Lambda_K^{-T}|| \leq Q_{K_2}$, $Q_B = \lambda_{min}(\Psi_B^T \Lambda_B^{-T})$, $||B_h^T \Psi_B^T \Lambda_B^{-T}|| \leq Q_{B_1}$, $||\dot{B}_h^T \Lambda_B^{-T}|| \leq Q_{B_2}$, $Q_\theta = \lambda_{min}(\Psi_\theta^T \Lambda_\theta^{-T})$, $||\theta_x^T \Psi_\theta^T \Lambda_\theta^{-T}|| \leq Q_{\theta_1}$, $Q_\eta = \lambda_{min}(\Psi_\eta^T \Lambda_\eta^{-T})$, $||\eta_x^T \Psi_\eta^T \Lambda_\eta^{-T}|| \leq Q_{\eta_1}$ and $||\dot{\eta}_x^T \Lambda_\eta^{-T}|| + c\beta \leq Q_{\eta_2}$. Therefore, the Lyapunov function's time derivative is negative definite ($\dot{V}(t) < 0$) outside the following region:

$$\begin{aligned}
\|\epsilon_x\| &\leq \frac{-D_2 + \sqrt{D_2^2 + 4D_1 D_3}}{2D_1} = \mathscr{H}_1 \\
\left\|\tilde{f}_{ff}\right\| &\leq \frac{-D_5 + \sqrt{D_5^2 + 4D_4 D_6}}{2D_4} = \mathscr{H}_2 \\
\left\|\tilde{K}_h\right\| &\leq \frac{-D_8 + \sqrt{D_8^2 + 4D_7 D_9}}{2D_7} = \mathscr{H}_3 \\
\left\|\tilde{B}_h\right\| &\leq \frac{-D_{11} + \sqrt{D_{11}^2 + 4D_{10} D_{12}}}{2D_{10}} = \mathscr{H}_4 \\
\left\|\tilde{\theta}_x\right\| &\leq \frac{-D_{14} + \sqrt{D_{14}^2 + 4D_{13} D_{15}}}{2D_{13}} = \mathscr{H}_5 \\
\|\tilde{\eta}_x\| &\leq \frac{-D_{17} + \sqrt{D_{17}^2 + 4D_{16} D_{18}}}{2D_{16}} = \mathscr{H}_6
\end{aligned} \tag{26}$$

in which $D_1 = \sigma Q_M$, $D_2 = Q_f ||\tilde{f}_{ff}||^2 + Q_K ||\tilde{K}_h||^2 + Q_B ||\tilde{B}_h||^2 + Q_\theta ||\tilde{\theta}_x||^2 + Q_\eta ||\tilde{\eta}_x||^2 - Q_{f_1} ||\tilde{f}_{ff}|| - Q_{K_1} ||\tilde{K}_h|| - Q_{B_1} ||\tilde{B}_h|| - Q_{\theta_1} ||\tilde{\theta}_x|| - Q_{\eta_1} ||\tilde{\eta}_x||$, $D_3 = A_0 + Q_{f_2} ||\tilde{f}_{ff}|| + Q_{K_2} ||\tilde{K}_h|| + Q_{B_2} ||\tilde{B}_h|| + Q_{\eta_2} ||\tilde{\eta}_x||$, $D_4 = Q_f ||\epsilon_x||$, $D_5 = -Q_{f_1} ||\epsilon_x|| - Q_{f_2}$, $D_6 = A_\epsilon + A_0 + A_K + A_B + A_\theta + A_\eta$, $D_7 = Q_K ||\epsilon_x||$, $D_8 = -Q_{K_1} ||\epsilon_x|| - Q_{K_2}$, $D_9 = A_\epsilon + A_0 + A_f + A_B + A_\theta + A_\eta$, $D_{10} = Q_B ||\epsilon_x||$, $D_{11} = -Q_{B_1} ||\epsilon_x|| - Q_{B_2}$, $D_{12} = A_\epsilon + A_0 + A_f + A_K + A_\theta + A_\eta$, $D_{13} = Q_\theta ||\epsilon_x||$, $D_{14} = -Q_{\theta_1} ||\epsilon_x||$, $D_{15} = A_\epsilon + A_0 + A_f + A_K + A_B + A_\eta$, $D_{16} = Q_\eta ||\epsilon_x||$, $D_{17} = -Q_{\eta_1} ||\epsilon_x|| - Q_{\eta_2}$ and $D_{18} = A_\epsilon + A_0 + A_f + A_K + A_B + A_\theta$. According to (26), all trajectories converge to the compact set

$$\mathscr{S} = \Big\{ \Big(\epsilon_x,\, \tilde{f}_{ff},\, \tilde{K}_h,\, \tilde{B}_h,\, \tilde{\theta}_x,\, \tilde{\eta}_x\Big) : \|\epsilon_x\| \le \mathscr{H}_1 \wedge \left\|\tilde{f}_{ff}\right\| \le \mathscr{H}_2 \wedge \left\|\tilde{K}_h\right\| \le \mathscr{H}_3 \wedge \left\|\tilde{B}_h\right\| \le \mathscr{H}_4 \wedge \left\|\tilde{\theta}_x\right\| \le \mathscr{H}_5 \wedge \|\tilde{\eta}_x\| \le \mathscr{H}_6 \Big\} \quad (27)$$

within a finite time $T$ and remain there $\forall\, t \ge T$.

Based on the provided stability analysis above, the magnitude of positive definite Lyapunov function decreases outside the compact set obtained in Eq. (26) in terms of all variables defined in (18). Therefore, the convergence to this bounded region is demonstrated with dimensions related to the actual human limb's impedance and its variations ($f_{ff}$, $K_h$, $\dot{K}_h$, $B_h$, $\dot{B}_h$), robot model uncertainties and unmodeled disturbances ($\theta_x$, $\eta_x$ and $\dot{\eta}_x$). This ensures that the system response is UUB for the tracking and estimation errors in (26). As a result, the closed-loop human-robot interaction using the proposed adaptive impedance-varying controller is stable under the assumption of bounded model mismatch or disturbance $f_{unc}$ in (5). In addition, the slope factor $\beta$ of the function $\tanh(\epsilon_x/\beta)$ in the robust control law (11) would affect $A_0$ and $Q_{\eta 2}$ in $A_\eta$ defined in (25). Accordingly, the reduction of $\beta$ would shrink the size of the final compact zone (26) while increasing $\beta$ will result in the smoothness of the control effort. This compromise on the adjustment of $\beta$ was introduced in Section III-A.

## V. Experimental Studies

The proposed adaptive impedance-varying control scheme is evaluated practically through comprehensive experimental studies. For this purpose, the Quanser rehabilitation robot (Quanser Consulting Inc., Markham, Canada) was employed with two degrees of freedom (DOFs) designed for horizontal planar motions of the upper limb. The kinematics and dynamics of this robot were previously comprehensively presented and mathematically parameterized [65], [66] to execute the control laws and adaptation rules. The QUARC (Quanser Real-Time Control) environment was utilized as the control software in these experiments with 1 $k$Hz sampling rate.

### A. Resistive Environment-Robot Interaction

The proposed strategy was firstly evaluated via rendering a resistive force field by a stiff environment designed to have physical interaction with the robot (instead of human) and generate a time-varying interaction force in different directions. Employing this test bed, the controller performance was analyzed more systematically before involving human users (described in the next section). As illustrated in Fig. 2, a set of four springs were attached to the robot's end-effector and a moving target (trajectory) was followed using the proposed strategy. The robot position in the $x-y$ plane and the target location were demonstrated by the hollow red and solid blue circles, respectively, on a monitor. The left screen in Fig. 2 shows online variation of the robot's impedance parameters determined by the update rule (16).

The gain values in the proposed nonlinear control law (9) and the update rules (15), (16) and (17) utilized in this experimental assessment on the Quanser rehabilitation robot are listed in Table I. These values were determined by

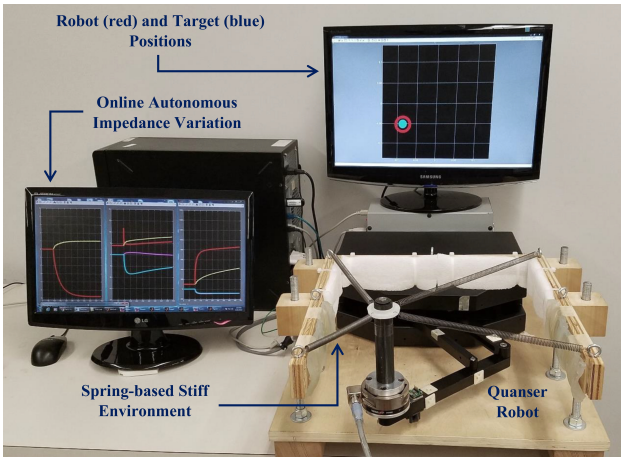


Fig. 2. Robotic set-up for the first experiments on the impedance-varying control strategy: Quanser rehabilitation robot attached to a spring-based stiff environment. The right monitor displays robot and desired (target) positions in the $x-y$ plane and the left monitor depicts the time-varying impedance components of the robot obtained from the adaptation law (16).

trial-and-error and performing initial experiments to achieve optimal tracking and flexibility performance of the pHRI system. Specifically, this gain adjustment led to a fast and smooth transient response in trajectory tracking and parameter adaptation as well as an appropriate convergence of the system's steady-state response to a bounded region (compact set) described in Section IV. The physical flexibility of the robot was analyzed to display enough deviation from the desired trajectory based on the human interaction by appropriate regulation of adaptation gains. For instance, increasing the update rate $\Psi_i$ in comparison with $\Lambda_i$ ($i = K, B, f$) in the adaptation rules (15), (16), and (17) results in the reduction of the estimated impedance elements. This would further relax the control effort (10) by providing more weight to the flexibility rather than tracking convergence. This compromise was explained in Section III-C and the flowchart of gain tuning for the control and adaptation laws is presented in Fig. 3. Note that the increments mentioned in this flow diagram were applied gradually and can be selected based on the initial gain values and the employed robotic system. The parameter $\beta$ was chosen to be 0.001 to have a large enough slope for the function $\tanh(\epsilon_x/\beta)$ in (11) around $\epsilon_x = 0$ with adequate similarity to $\mathrm{sgn}(\epsilon_x)$ as discussed in Section III-A. However, the chattering issue in the control effort was avoided during the convergence of closed-loop response due to the continuity of tanh function. In this condition and having $c = 0.2785$ in (21), the magnitude of $c\beta = 0.0002785$ in (25) is very small and negligible relative to the size of the final compact set (26).

The Cartesian position of the robot end-effector in the $x-y$ plane is illustrated in Fig. 4. The robot response converged to the vicinity of the desired target after adequate time. This performance can be better seen in Fig. 5, which depicts the tracking error $e_x$ in the $x$ and $y$ directions, which approached values less than 2 mm after 100 s of the robot interaction with the environment (1% of 20 cm motion range). This convergence of the tracking error to a small bounded region is due to the controller's design and the adaptation of

| Rules | Control Law (7) | Adapt Laws (15) & (17) | Adapt Law (16) |
|---|---|---|---|
| Gains | $\sigma = 150$, $\zeta = 16$ | $\Lambda_\theta = 42\,I$, $\Psi_\theta = 30\,I$, $\Lambda_\eta = 2.5\,I$, $\Psi_\eta = 1.8\,I$ | $\Lambda_K = 500\,I$, $\Psi_K = 350\,I$, $\Lambda_B = 40\,I$, $\Psi_B = 32\,I$, $\Lambda_f = 0.5\,I$, $\Psi_f = 0.4\,I$ |

$I$: Identity matrix

TABLE I
EMPLOYED GAIN VALUES IN EXPERIMENTAL IMPLEMENTATION OF THE PROPOSED CONTROL AND ADAPTATION LAWS

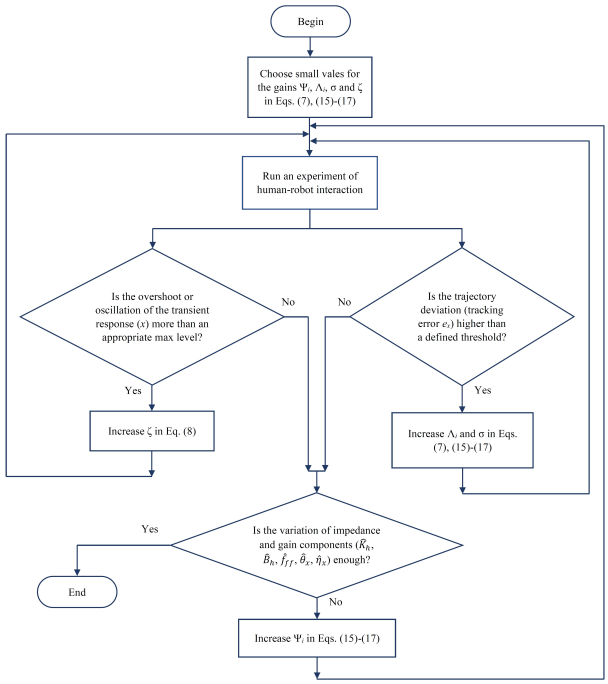


Fig. 3. Flow diagram of gain tuning for the control and adaptation laws (7), (15)-(17) by performing initial experiments

robot impedance, dynamic parameters and the robust SMC gain during the interaction task, as proven in Section IV. The convergence rate can be regulated based on any task requirements through the simultaneous regulation of control and adaptation gains.

The autonomous variation of impedance components is shown in Fig. 6 for the stiffness $\hat{K}_h$, damping $\hat{B}_h$ and feedforward force $\hat{f}_{ff}$. These values were acquired online from the update rule (16) and transformed to the Normal-Tangential (N-T) coordinates relative to the circular motion path. Note that the normal and tangential axes are perpendicular and parallel to the concurrent tangent of the target trajectory, respectively. These results imply that the adaptive impedance parameters remain bounded relative to the actual human limb impedance ($K_h$, $B_h$ and $f_{ff}$), as analyzed in Section IV. Moreover, this adaptation (16) was able to estimate the main mechanical properties of the environment such as its main stiffness elements and feedfoward forces. Accordingly, the maximum stiffness element in Fig. 6(a) was approximated as $\hat{K}_{h_{22}} \approx 65$ N/m in the normal direction, which is perpendicular to the trajectory and toward the center of 2D space (the rest configuration in

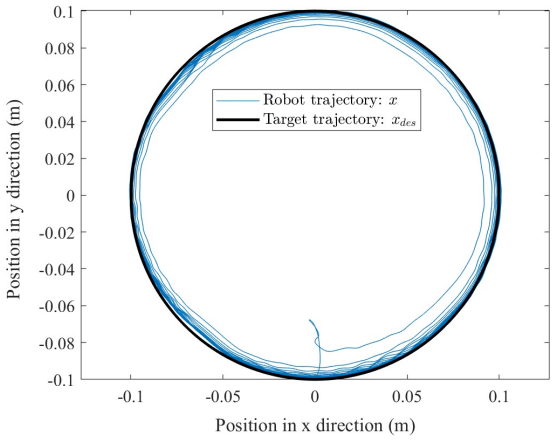


Fig. 4. Cartesian position trajectory of the robot end-effector in $x-y$ plane relative to the desired moving target trajectory

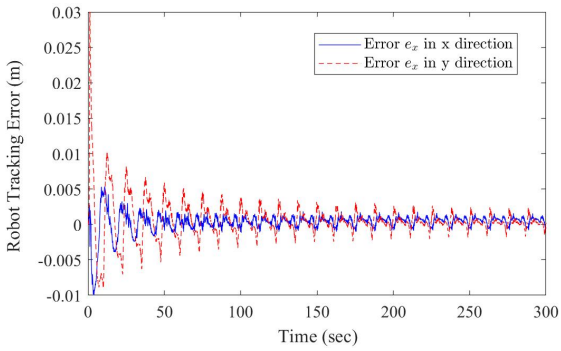


Fig. 5. Convergence of the tracking error in $x$ and $y$ directions to a bounded small value (less than 2 mm in each direction)

the springs set). Also, the major feedforward force $f_{ff_2}$ was in the same normal direction as demonstrated in Fig. 6(c), which was estimated around 6 N due to 0.1 m deflection of the spring-based setup toward the circular path of motion in Fig. 4. Therefore, the proposed impedance adaptation (16) could approximate the environment's physical characteristics and adjust the robot impedance accordingly.

For further comparative analysis, a previous impedance-varying strategy proposed in [44] was implemented with the same resistive force field (Fig. 2) and circular trajectory. The same approach was employed to adjust the gains of this controller as the one introduced at the beginning of this section and demonstrated in Fig. 3. The system response using the previous strategy [44] in following the desired trajectory and interacting with the stiff environment is illustrated in Fig. 7(a) and the corresponding tracking error is shown in Fig. 7(b). As seen, a considerable deviation (more than 0.01 m) was achieved in both the $x$ and $y$ directions toward the origin due to the force of the springs. This was five times larger than the steady-state amplitude of the deviation obtained using the proposed scheme demonstrated in Figs. 4 and 5. This larger deviation using the previous method [44] is due to the lack of consideration of robot and environment uncertainties. The result of impedance variation suggested in [44] for adjusting the robot stiffness components is depicted in Fig. 7(c), which are transformed to the N-T coordinates. Considering

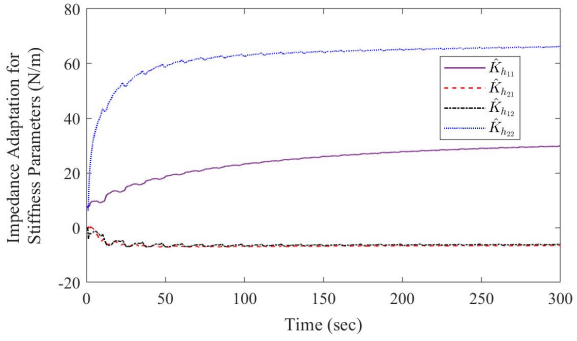


(a)

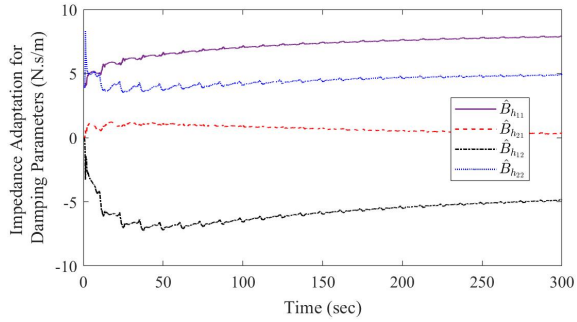


(b)

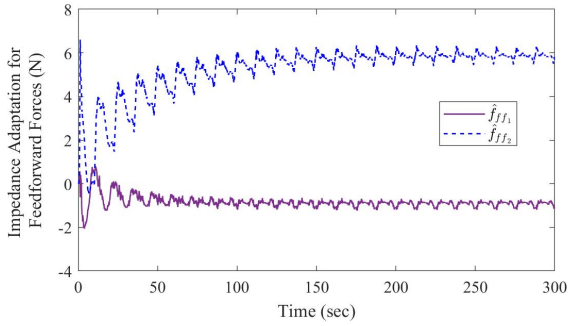


(c)

Fig. 6. Autonomous variation of impedance parameters: (a) stiffness $\hat{K}_h$, (b) damping $\hat{B}_h$ and (c) feedforward force $\hat{f}_{ff}$ based on the update rule (16), which are transformed to the Normal-Tangential coordinates

the stationary environment stiffness, this performance implies the lack of convergence to specific steady-state values that we achieved (Fig. 6(a)) by employing the proposed impedance-varying scheme. Overall, significant changes in the impedance regulation in response to the external force and ignoring unstructured uncertainties of the system in [44] resulted in larger deviations from the desired trajectory in comparison with the performance of the proposed impedance-varying control strategy.

### *B. Human-Robot Interaction*

In this experiment, a human operator grasped the robot's end-effector handle and a moving target (trajectory) was followed by implementing the proposed autonomous controller for pHRI. As shown in Fig. 8, the user can observe his/robot position in the $x-y$ plane with respect to the target location demonstrated on the right screen. Online variations of the

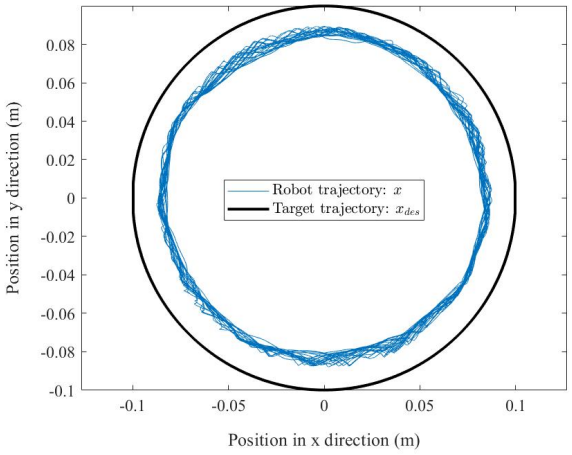


(a)

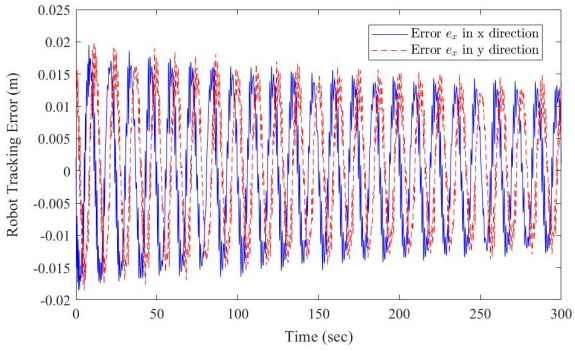


(b)

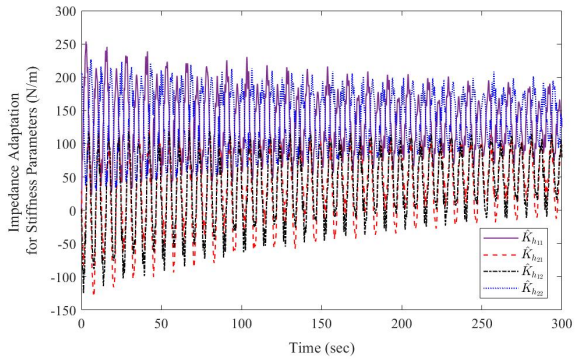


(c)

Fig. 7. Response of a previous impedance-varying method [44]: (a) position trajectory of the robot in following a circular trajectory in Cartesian coordinates, (b) tracking error (deviation) $e_x$, and (c) variation of the robot stiffness $\hat{K}_h$ transformed to the N-T space

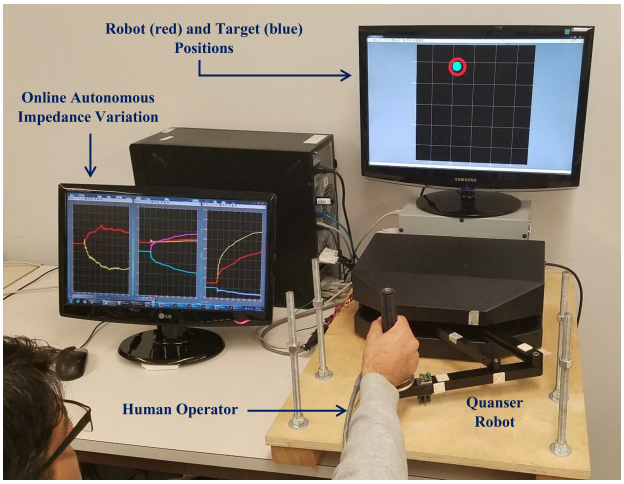


Fig. 8. Robotic interface for the second experiment on the impedance-varying control strategy: Quanser rehabilitation robot interacting with a human operator. The right monitor displays robot and desired (target) positions in the $x-y$ plane and the left monitor depicts the time-varying impedance components of the robot determined from the adaptation law (16).

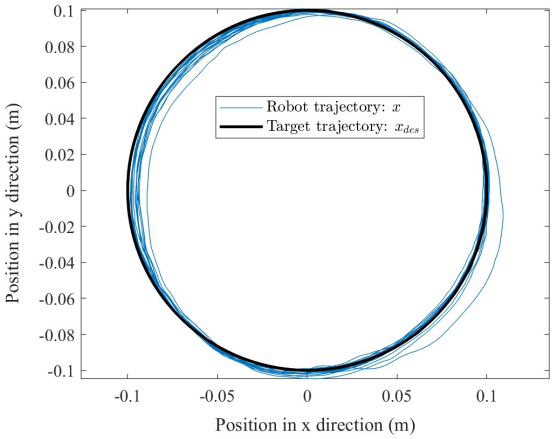


Fig. 9. Human/robot motion in $x-y$ Cartesian coordinates relative to the desired target trajectory

robot's impedance parameters are also illustrated by the screen on the left side of Fig. 8.

The robot-handle/human-hand trajectory in 2D space is represented in Fig. 9. The bounded convergence of this pHRI response ($x$) to the target motion ($x_{des}$) was achieved, although the human operator deviates outside and inside of the desired trajectory due to his interaction behavior. These deviations were larger at the beginning of the interaction before thet adequate adaptation of the robot impedance to the operator's impedance was achieved. This performance can be better observed in the time history of the tracking error $e_x$, which converged to a bounded region, with less than 2.5 mm amplitude in each of the $x$ and $y$ directions of the Cartesian coordinates (1.25% of 20 cm motion range), as depicted in Fig. 10.

This outcome was attained as a result of estimating human impedance by the adaptation law (16). The online variation of these impedance components are illustrated in Fig. 11(c). Similar to the previous set of experiments, levels of appropriate stiffness and damping elements ($\hat{K}_h$ and $\hat{B}_h$) for the robot

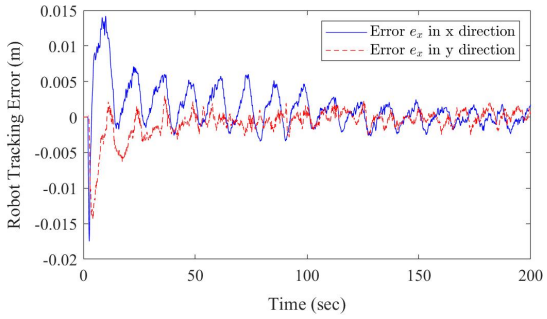


Fig. 10. Bounded convergence of the tracking error in $x$ and $y$ coordinates (with a final bound less than 2.5 mm in each direction)

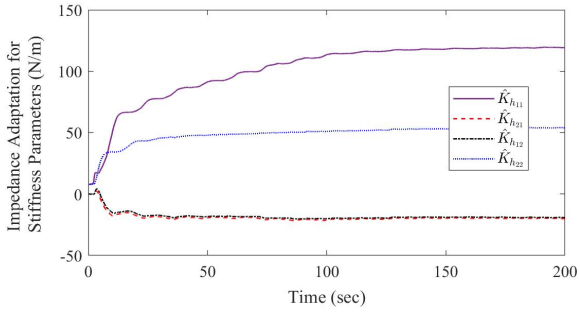


(a)

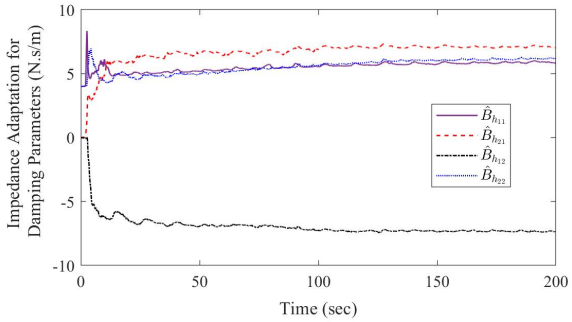


(b)

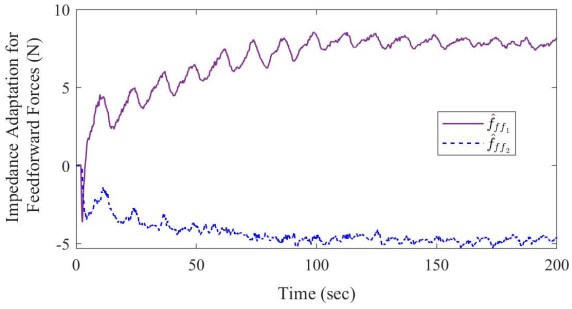


(c)

Fig. 11. Autonomous estimation of desired impedance parameters in physical human-robot interaction (pHRI): (a) stiffness $\hat{K}_h$, (b) damping $\hat{B}_h$ and (c) feedforward force $\hat{f}_{ff}$ based on the update rule (16)

were found after a short period of interaction with the human, and the rest of the interaction force was treated as the feedforward force $\hat{f}_{ff}$ based on the modeling and control of the interaction force in (4) and (10).

To assess the estimated pHRI force, direct force measurement was obtained in these experiments using an ATI Gamma F/T sensor (ATI Industrial Automation, Apex, USA) attached

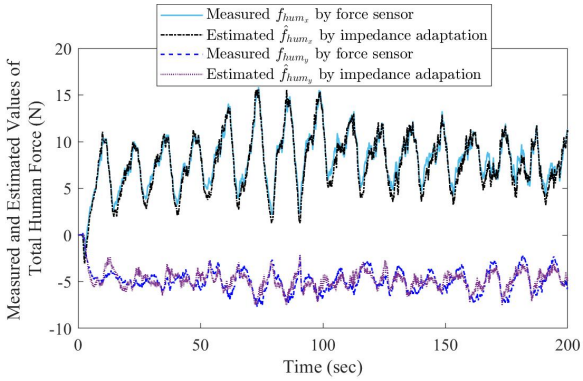


Fig. 12. Measured value of the interaction force $f_{hum}$ and its estimation as the summation of estimated stiffness-based and damping-based and feedforward forces based on Eq. (4) in $x$ and $y$ directions

to the robot end-effector. This measured force was not employed in the controller's structure and it was only obtained for the evaluation of the proposed impedance adaptation strategy. The summation of estimated stiffness-based, damping-based and feedforward forces based on Eq. (4) is shown in Fig. 12 together with the measured value of the interaction force $f_{hum}$. The designed adaptation (16) of the impedance elements resulted in accurate estimation of the actual pHRI force (with less than 1 N error), even though it was highly time-varying and dependent on the human arm posture along the motion trajectory. Since this user applied forces mostly toward the $+x$ and $-y$ directions (shown in Figs. 11(c) and 12), the robot showed flexibility and deviated toward the right and bottom relative to the target trajectory in 2D space (see Fig. 9).

It is worth mentioning that the small error in the human force estimation and modeling mismatch in the robot dynamics were considered by $f_{unc}$ in Eqs. (2) and (5). The proposed controller was made robust against these uncertainties by the designed adaptation law (17) for the sliding-mode gain $\hat{\eta}_x$, as proven in Section IV. The online variation and the final value of this gain vector can be observed in Fig. 13. Based on the stability analysis in Section IV, this robust gain's adaptation together with the adaptation for the impedance and robot parameters as well as the control laws resulted in pHRI stability and boundedness of tracking and estimation errors. The oscillations seen in the closed-loop system's response were due to the tracking of repetitive trajectories of the motion and fluctuation of the error around zero, and not because of the chattering phenomenon. The chattering was avoided by employing a hyperbolic tangent function instead of the discontinuous sign function in the robust term (11). To investigate this point further, the control effort $f_{con}$ generated by the proposed strategy (6) in this experiment (Fig. 9) is shown in Fig. 14. As two time periods with high variations were focused on Fig. 14, no high-frequency chattering occurred for the command control signals.

To elaborate more on the performance of the proposed controller, the tracking and adaptation features of this strategy were evaluated for a triangle trajectory, demonstrated in Fig. 15. The sharp corners of this trajectory and the resulting sudden changes in the motion velocity and acceleration affected the physical interaction between the robot and human. As a

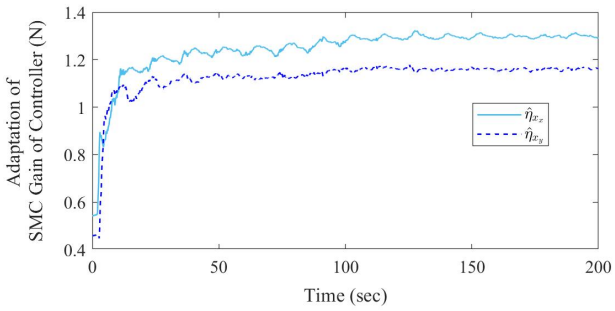


Fig. 13. Online variation of the sliding-mode gain $\hat{\eta}_x$ to make the controlled HRI robust against human force estimation error and modeling mismatch in the robot dynamics using (17)

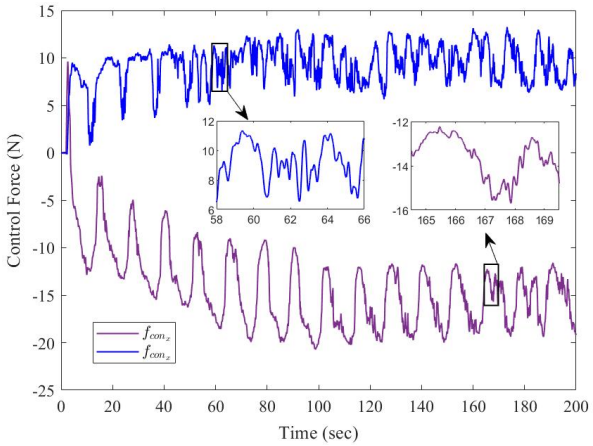


Fig. 14. Control force $f_{con}$ generated by the proposed strategy (6) for the HRI shown in Fig. 9

result, the peaks of tracking errors in Fig. 16 occurred at these moments of the trajectory corners.

Due to these sudden variations of the motion and corresponding errors, the estimation of human feedforward force experienced sudden jumps, as shown in Fig. 17, compared to the previous circular motion in Fig. 11(c). Some of these jumps are highlighted by black circles; however, an appropriate estimation of the human force with convergence to certain

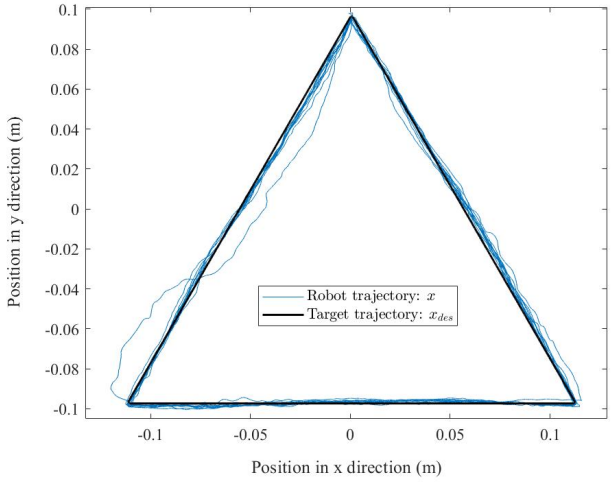


Fig. 15. Triangular reference trajectory with rounded edges in $x-y$ Cartesian coordinates and human/robot response motion

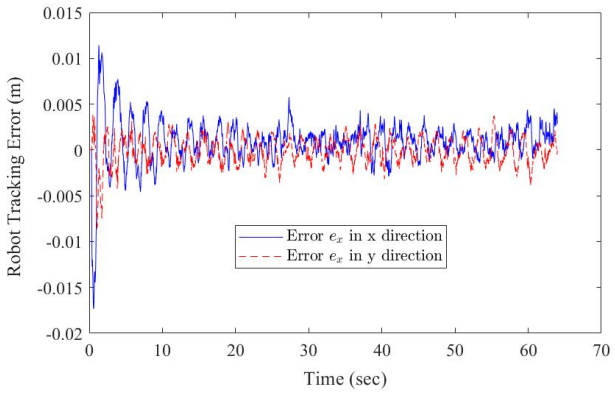


Fig. 16. Convergence of the tracking error with a final bound less than 5 mm in each of $x$ and $y$ directions

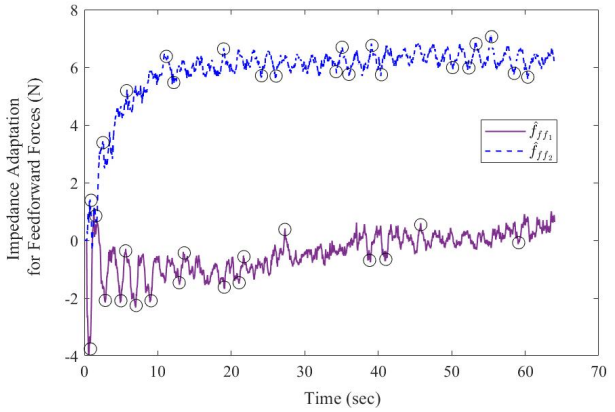


Fig. 17. Estimation of the human feedforward force $\hat{f}_{ff}$ in tracking a triangular trajectory

levels is seen in a broader view. Moreover, the estimation of the controller's robust gain vector $\hat{\eta}_x$ for this triangular motion is illustrated in Fig. 18. The adjustment of this gain's components according to the update rule (17) also had some sharp oscillations because of the jumps in the tracking error (Fig. 16) due to the variation of HRI with a high-curvature trajectory (Fig. 15). While some peaks occurred in the robust gains at the beginning of this interaction in following the triangular trajectory (depicted by black circles in Fig. 18) compared to the previous case (Fig. 13), the proposed intelligent adaptation law was able to approximate the required level of these gains during the first 20 sec of the motion.

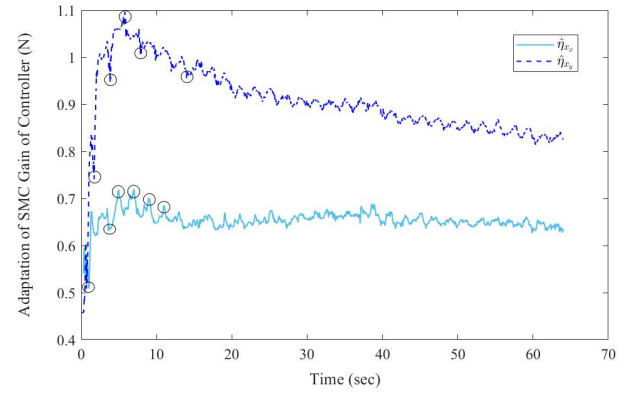


Fig. 18. Adjustment of the robust gain $\hat{\eta}_x$ based on (17) in the case of triangular movement

Note that the magnitudes of $\Lambda_i$ and $\Psi_i$ in any of adaptation laws (15), (16) and (17) affects the magnitude of the tracking error ($\epsilon_x$) and robot behavior, as discussed in Section III-C and analyzed in Section IV. For instance, by relaxing $\Lambda_i$ and raising $\Psi_i$ in these variation rules, the robot becomes more flexible physically for the human and higher deviation levels are admitted.

## VI. Concluding Remarks

In this study, a nonlinear impedance-varying control method was developed for an intelligent pHRI. This autonomous strategy facilitated a stable collaboration between the robot and the human considering their modeling uncertainties, and without employing any measurement of interaction force. New update rules were defined for the online estimation of the human impedance components (stiffness and damping matrices) and human feedforward force. Another adaptation law was formulated to estimate the robot dynamic parameters. Moreover, a variation scenario was designed for the SMC gain to overcome mismatch and disturbances in the pHRI model.

Stability of the robotic system using the proposed controller, in terms of the UUB of the tracking error and the estimation errors of human and robot parameters, was proven using a comprehensive Lyapunov analysis. In this regard, a compromise between tracking convergence and physical flexibility of the robot was addressed. Deviation from the desired pHRI task trajectory remained bounded while the human impedance and robot dynamics parameters and the appropriate controller's gain were estimated with bounded errors.

Experimental studies were carried out using the Quanser robot to evaluate the performance of the proposed autonomous impedance-varying controller, where a resistive spring-based environment and a human operator were involved. Suitable fast adjustment of the robot impedance and the controller's robust gain based on the interaction with the human/environment was achieved to ensure stability while converging to a small bounded vicinity of the target trajectory (less than 2% of the motion range). The proposed autonomous impedance adaptation rule was capable of estimating the environment's stiffness and feedforward forces. In addition, the obtained online approximation for the total pHRI interaction force through this impedance adaptation had high accuracy in comparison with the measured force.

This control strategy can be utilized in various pHRI tasks such as autonomous movement therapies, assistive exoskeletons and surgery operations where no force sensors are augmented to the robot. In future work, more sophisticated (higher- or fractional- order) dynamical systems can be considered for the human limb interacting with the robot to model more biomechanical details in various applications. The proposed impedance learning method can also be extended for more complex robotic systems such as tele-robotic systems including two or more robots communicating with each other and interacting with different human operators and/or environments.

## Acknowledgment

This work was supported by the Natural Sciences and Engineering Research Council, Canadian Institutes of Health

Research, Canada Foundation for Innovation, and the Government of Alberta. VKM is a Canada Research Chair (Tier 1) in Functional Restoration. MS is a recipient of a postdoctoral fellowship award from the SMART Network Innovation Fund.

## REFERENCES


[1] M. Sharifi, S. Behzadipour, and G. Vossoughi, "Nonlinear model reference adaptive impedance control for human–robot interactions," *Control Engineering Practice*, vol. 32, pp. 9 – 27, 2014.

[2] A. Bicchi, M. A. Peshkin, and J. E. Colgate, *Safety for Physical Human–Robot Interaction*. Berlin, Heidelberg: Springer Berlin Heidelberg, 2008, pp. 1335–1348.

[3] S. Haddadin and E. Croft, *Physical Human–Robot Interaction*. Cham: Springer International Publishing, 2016, pp. 1835–1874.

[4] N. Hogan, "Impedance Control: An Approach to Manipulation: Part I theory; Part II implementation; Part III applications," *Journal of Dynamic Systems, Measurement, and Control*, vol. 107, no. 1, pp. 1–24, 1985.

[5] H. Kazerooni, T. Sheridan, and P. Houpt, "Robust compliant motion for manipulators, part i: The fundamental concepts of compliant motion," *IEEE Journal on Robotics and Automation*, vol. 2, no. 2, pp. 83–92, 1986.

[6] M. Sharifi, A. Zakerimanesh, J. K. Mehr, A. Torabi, V. K. Mushahwar, and M. Tavakoli, "Impedance variation and learning strategies in human-robot interaction," *IEEE Transactions on Cybernetics*, pp. 1–14, 2021.

[7] F. Aghili, "Robust impedance-matching of manipulators interacting with uncertain environments: Application to task verification of the space station's dexterous manipulator," *IEEE/ASME Transactions on Mechatronics*, vol. 24, no. 4, pp. 1565–1576, 2019.

[8] D. Kim, K. Koh, G. Cho, and L. Zhang, "A robust impedance controller design for series elastic actuators using the singular perturbation theory," *IEEE/ASME Transactions on Mechatronics*, vol. 25, no. 1, pp. 164–174, 2020.

[9] R. J. Anderson and M. W. Spong, "Hybrid impedance control of robotic manipulators," *IEEE Journal on Robotics and Automation*, vol. 4, no. 5, pp. 549–556, 1988.

[10] A. Abdossalami and S. Sirouspour, "Adaptive control for improved transparency in haptic simulations," *IEEE Transactions on Haptics*, vol. 2, no. 1, pp. 2–14, 2009.

[11] N. Hogan, "Adaptive control of mechanical impedance by coactivation of antagonist muscles," *IEEE Transactions on Automatic Control*, vol. 29, no. 8, pp. 681–690, 1984.

[12] R. Ikeura, H. Monden, and H. Inooka, "Cooperative motion control of a robot and a human," in *Proceedings of IEEE International Workshop on Robot and Human Communication*, 1994, pp. 112–117.

[13] M. M. Rahman, R. Ikeura, and K. Mizutani, "Investigating the impedance characteristic of human arm for development of robots to co-operate with human operators," in *IEEE International Conference on Systems, Man, and Cybernetics*, 1999, pp. 676–681.

[14] V. Duchaine, B. Mayer St-Onge, D. Gao, and C. Gosselin, "Stable and intuitive control of an intelligent assist device," *IEEE Transactions on Haptics*, vol. 5, no. 2, pp. 148–159, 2012.

[15] S. P. Buerger and N. Hogan, "Complementary stability and loop shaping for improved human-robot interaction," *IEEE Transactions on Robotics*, vol. 23, no. 2, pp. 232–244, 2007.

[16] Q. Wei, Z. Li, K. Zhao, Y. Kang, and C. Su, "Synergy-based control of assistive lower-limb exoskeletons by skill transfer," *IEEE/ASME Transactions on Mechatronics*, vol. 25, no. 2, pp. 705–715, 2020.

[17] I. Ranatunga, F. L. Lewis, D. O. Popa, and S. M. Tousif, "Adaptive admittance control for human–robot interaction using model reference design and adaptive inverse filtering," *IEEE Transactions on Control Systems Technology*, vol. 25, no. 1, pp. 278–285, 2017.

[18] K. Lee and M. Buss, "Force tracking impedance control with variable target stiffness," *Proceedings of 17th IFAC World Congress*, vol. 41, no. 2, pp. 6751 – 6756, 2008.

[19] T. Zhang, M. Tran, and H. Huang, "Admittance shaping-based assistive control of sea-driven robotic hip exoskeleton," *IEEE/ASME Transactions on Mechatronics*, vol. 24, no. 4, pp. 1508–1519, 2019.

[20] H. P. Huang and S. S. Chen, "Compliant motion control of robots by using variable impedance," *The International Journal of Advanced Manufacturing Technology*, vol. 7, no. 6, pp. 322–332, 1992.

[21] F. Ficuciello, L. Villani, and B. Siciliano, "Variable impedance control of redundant manipulators for intuitive human–robot physical interaction," *IEEE Transactions on Robotics*, vol. 31, no. 4, pp. 850–863, 2015.

[22] R. Ikeura, T. Moriguchi, and K. Mizutani, "Optimal variable impedance control for a robot and its application to lifting an object with a human," in *Proceedings of IEEE International Workshop on Robot and Human Interactive Communication*, 2002, pp. 500–505.

[23] A. Lecours, B. Mayer-St-Onge, and C. Gosselin, "Variable admittance control of a four-degree-of-freedom intelligent assist device," in *IEEE International Conference on Robotics and Automation*, 2012, pp. 3903–3908.

[24] R. V. Dubey, Tan Fung Chan, and S. E. Everett, "Variable damping impedance control of a bilateral telerobotic system," *IEEE Control Systems Magazine*, vol. 17, no. 1, pp. 37–45, 1997.

[25] C. Mitsantisuk, K. Ohishi, and S. Katsura, "Variable mechanical stiffness control based on human stiffness estimation," in *IEEE International Conference on Mechatronics*, 2011, pp. 731–736.

[26] M. S. Erden and A. Billard, "Robotic assistance by impedance compensation for hand movements while manual welding," *IEEE transactions on cybernetics*, vol. 46, no. 11, pp. 2459–2472, 2015.

[27] M. S. Erden and B. Marić, "Assisting manual welding with robot," *Robotics and Computer-Integrated Manufacturing*, vol. 27, no. 4, pp. 818–828, 2011.

[28] D. Surdilovic and Z. Cojbasic, "Robust robot compliant motion control using intelligent adaptive impedance approach," in *IEEE International Conference on Robotics and Automation (ICRA)*, vol. 3, 1999, pp. 2128–2133.

[29] H. Kazerooni, "Automated robotic deburring using impedance control," *IEEE Control Systems Magazine*, vol. 8, no. 1, pp. 21–25, 1988.

[30] L. Roveda, N. Pedrocchi, M. Beschi, and L. M. Tosatti, "High-accuracy robotized industrial assembly task control schema with force overshoots avoidance," *Control Engineering Practice*, vol. 71, pp. 142–153, 2018.

[31] M. Sharifi, H. Salarieh, S. Behzadipour, and M. Tavakoli, "Beating-heart robotic surgery using bilateral impedance control: Theory and experiments," *Biomedical signal processing and control*, vol. 45, pp. 256–266, 2018.

[32] A. Taherifar, G. Vossoughi, and A. Selk Ghafari, "Optimal target impedance selection of the robot interacting with human," *Advanced Robotics*, vol. 31, no. 8, pp. 428–440, 2017.

[33] M. Sharifi, J. K. Mehr, V. K. Mushahwar, and M. Tavakoli, "Adaptive cpg-based gait planning with learning-based torque estimation and control for exoskeletons," *IEEE Robotics and Automation Letters*, 2021.

[34] J. K. Mehr, M. Sharifi, V. K. Mushahwar, and M. Tavakoli, "Intelligent locomotion planning with enhanced postural stability for lower-limb exoskeletons," *IEEE Robotics and Automation Letters*, vol. 6, no. 4, pp. 7588–7595, 2021.

[35] A. Ajoudani, N. Tsagarakis, and A. Bicchi, "Tele-impedance: Teleoperation with impedance regulation using a body–machine interface," *The International Journal of Robotics Research*, vol. 31, no. 13, pp. 1642–1656, 2012.

[36] F. Ferraguti, N. Preda, A. Manurung, M. Bonfè, O. Lambercy, R. Gassert, R. Muradore, P. Fiorini, and C. Secchi, "An energy tank-based interactive control architecture for autonomous and teleoperated robotic surgery," *IEEE Transactions on Robotics*, vol. 31, no. 5, pp. 1073–1088, 2015.

[37] F. Ferraguti, C. Secchi, and C. Fantuzzi, "A tank-based approach to impedance control with variable stiffness," in *IEEE International Conference on Robotics and Automation (ICRA)*, 2013, pp. 4948–4953.

[38] A. Zakerimanesh, M. Sharifi, F. Hashemzadeh, and M. Tavakoli, "Delay-robust nonlinear control of bounded-input telerobotic systems with synchronization enhancement," *IEEE Robotics and Automation Letters*, vol. 6, no. 2, pp. 2493–2500, 2021.

[39] E. Spyrakos-Papastavridis, P. R. N. Childs, and J. S. Dai, "Passivity preservation for variable impedance control of compliant robots," *IEEE/ASME Transactions on Mechatronics*, 2019.

[40] K. Kronander and A. Billard, "Stability considerations for variable impedance control," *IEEE Transactions on Robotics*, vol. 32, no. 5, pp. 1298–1305, 2016.

[41] T. Sun, L. Peng, L. Cheng, Z. Hou, and Y. Pan, "Stability-guaranteed variable impedance control of robots based on approximate dynamic inversion," *IEEE Transactions on Systems, Man, and Cybernetics: Systems*, pp. 1–8, 2019.

[42] Y. Dong and B. Ren, "Ude-based variable impedance control of uncertain robot systems," *IEEE Transactions on Systems, Man, and Cybernetics: Systems*, 2017.

[43] Q. C. Zhong and D. Rees, "Control of uncertain lti systems based on an uncertainty and disturbance estimator," *Journal of dynamic systems, measurement, and control*, vol. 126, no. 4, pp. 905–910, 2004.

[44] C. Yang, G. Ganesh, S. Haddadin, S. Parusel, A. Albu-Schaeffer, and E. Burdet, "Human-like adaptation of force and impedance in stable and

unstable interactions," *IEEE Transactions on Robotics*, vol. 27, no. 5, pp. 918–930, 2011.
[45] Z. Li, J. Liu, Z. Huang, Y. Peng, H. Pu, and L. Ding, "Adaptive impedance control of human–robot cooperation using reinforcement learning," *IEEE Transactions on Industrial Electronics*, vol. 64, no. 10, pp. 8013–8022, 2017.
[46] G. Ganesh, N. Jarrassé, S. Haddadin, A. Albu-Schaeffer, and E. Burdet, "A versatile biomimetic controller for contact tooling and haptic exploration," in *IEEE International Conference on Robotics and Automation*, 2012, pp. 3329–3334.
[47] J. Fong and M. Tavakoli, "Kinesthetic teaching of a therapist's behavior to a rehabilitation robot," in *2018 International Symposium on Medical Robotics (ISMR)*, 2018, pp. 1–6.
[48] L. Rozo, S. Calinon, D. G. Caldwell, P. Jimenez, and C. Torras, "Learning physical collaborative robot behaviors from human demonstrations," *IEEE Transactions on Robotics*, vol. 32, no. 3, pp. 513–527, 2016.
[49] S. Calinon, D. Bruno, and D. G. Caldwell, "A task-parameterized probabilistic model with minimal intervention control," in *IEEE International Conference on Robotics and Automation (ICRA)*, 2014, pp. 3339–3344.
[50] S. Schaal, P. Mohajerian, and A. Ijspeert, "Dynamics systems vs. optimal control—a unifying view," *Progress in brain research*, vol. 165, pp. 425–445, 2007.
[51] A. J. Ijspeert, J. Nakanishi, H. Hoffmann, P. Pastor, and S. Schaal, "Dynamical movement primitives: Learning attractor models for motor behaviors," *Neural Computation*, vol. 25, no. 2, pp. 328–373, 2013.
[52] C. Yang, C. Zeng, P. Liang, Z. Li, R. Li, and C. Su, "Interface design of a physical human–robot interaction system for human impedance adaptive skill transfer," *IEEE Transactions on Automation Science and Engineering*, vol. 15, no. 1, pp. 329–340, 2018.
[53] C. Yang, C. Zeng, C. Fang, W. He, and Z. Li, "A dmps-based framework for robot learning and generalization of humanlike variable impedance skills," *IEEE/ASME Transactions on Mechatronics*, vol. 23, no. 3, pp. 1193–1203, 2018.
[54] C. Yang, C. Zeng, Y. Cong, N. Wang, and M. Wang, "A learning framework of adaptive manipulative skills from human to robot," *IEEE Transactions on Industrial Informatics*, vol. 15, no. 2, pp. 1153–1161, 2019.
[55] Y. Li and S. S. Ge, "Impedance learning for robots interacting with unknown environments," *IEEE Transactions on Control Systems Technology*, vol. 22, no. 4, pp. 1422–1432, 2014.
[56] S. S. Ge, Y. Li, and C. Wang, "Impedance adaptation for optimal robot–environment interaction," *International Journal of Control*, vol. 87, no. 2, pp. 249–263, 2014.
[57] R. Yang, C. Yang, M. Chen, and J. Na, "Adaptive impedance control of robot manipulators based on q-learning and disturbance observer," *Systems Science & Control Engineering*, vol. 5, no. 1, pp. 287–300, 2017.
[58] X. Liu, S. S. Ge, F. Zhao, and X. Mei, "Optimized impedance adaptation of robot manipulator interacting with unknown environment," *IEEE Transactions on Control Systems Technology*, pp. 1–9, 2020.
[59] Y. Li, G. Ganesh, N. Jarrassé, S. Haddadin, A. Albu-Schaeffer, and E. Burdet, "Force, impedance, and trajectory learning for contact tooling and haptic identification," *IEEE Transactions on Robotics*, vol. 34, no. 5, pp. 1170–1182, 2018.
[60] G. Ganesh, A. Albu-Schäffer, M. Haruno, M. Kawato, and E. Burdet, "Biomimetic motor behavior for simultaneous adaptation of force, impedance and trajectory in interaction tasks," in *IEEE International Conference on Robotics and Automation (ICRA)*, 2010, pp. 2705–2711.
[61] O. Khatib, "A unified approach for motion and force control of robot manipulators: The operational space formulation," *IEEE Journal on Robotics and Automation*, vol. 3, no. 1, pp. 43–53, 1987.
[62] J. Slotine and W. Li, *Applied Nonlinear Control*, ser. Prentice-Hall International Editions. Prentice-Hall, 1991.
[63] M. Sharifi, "Impedance control of non-linear multi-dof teleoperation systems with time delay: absolute stability," *IET Control Theory Applications*, vol. 12, pp. 1722–1729(7), 2018.
[64] M. M. Polycarpou and P. A. Ioannou, "A robust adaptive nonlinear control design," in *American Control Conference*, 1993, pp. 1365–1369.
[65] M. Dyck and M. Tavakoli, "Measuring the dynamic impedance of the human arm without a force sensor," in *IEEE 13th International Conference on Rehabilitation Robotics (ICORR)*, 2013, pp. 1–8.
[66] M. D. Dyck, "Measuring the dynamic impedance of the human arm," Master Thesis, University of Alberta, 2013.

**Mojtaba Sharifi** is a postdoctoral research fellow in the Department of Electrical and Computer Engineering and the Department of Medicine, University of Alberta, Canada. He received his B.Sc. and M.Sc. degrees in Mechanical Engineering from Shiraz University and Sharif University of Technology, Iran, in 2010 and 2012, respectively. He conducted a collaborative research project in the Telerobotic and Biorobotic Systems Lab of the University of Alberta, Canada, from 2015 to 2016, and earned his Ph.D. degree from Sharif University of Technology, Iran, in 2017. His interdisciplinary research includes control, dynamics and design of robots (in biomedical applications: rehabilitation, surgery and imaging), human-robot interaction (using impedance control and learning), haptics, collaborative robotics and tele-robotics (using bilateral and multilateral control), wearable and assistive robotics (exoskeleton, prosthesis and orthosis), control and modeling of musculoskeletal systems, and biological systems.

**Vahid Azimi** received the Ph.D. degree in electrical engineering (systems and controls) from the Georgia Institute of Technology, Atlanta, GA, USA, in 2020. He is currently a Postdoctoral Research Fellow in the Stanford Energy Control Lab at Stanford University, Stanford, CA, USA. His current work focuses on modeling, control, and optimization of large scale systems, with special emphasis on high energy Li-ion battery packs. His research interests center on nonlinear control systems, optimization, energy systems, and robotics. From 2014 to 2016, he was a Researcher at the Cleveland State University, Cleveland, OH, USA (ECSR Lab), and the Georgia Institute of Technology (AMBER Lab).

**Vivian K. Mushahwar** received her B.Sc. degree in electrical engineering from Brigham Young University, Provo, UT, USA in 1991 and a Ph.D. degree in bioengineering from the University of Utah, Salt Lake City, USA in 1996. She received postdoctoral training at Emory University, Atlanta, GA, USA and the University of Alberta, Edmonton, AB, Canada. She is currently a professor in the Department of Medicine, Division of Physical Medicine and Rehabilitation at the University of Alberta, a Canada Research Chair (Tier 1) in Functional Restoration, and a Killam Professor. She is also the director of the Sensory Motor Adaptive Rehabilitation Technology (SMART) Network at the University of Alberta. Her research interests include identification of spinal-cord systems involved in locomotion, development of spinal-cord-based neural prostheses for restoring mobility after spinal cord injury, identification of rehabilitation interventions for enhancing mobility, and the use of active intelligent wearable devices for preventing secondary complications associated with neurological conditions including spasticity, pressure injuries, and deep vein thrombosis.

**Mahdi Tavakoli** is a Professor in the Department of Electrical and Computer Engineering, University of Alberta, Canada. He received his BSc and MSc degrees in Electrical Engineering from Ferdowsi University and K.N. Toosi University, Iran, in 1996 and 1999, respectively. He received his PhD degree in Electrical and Computer Engineering from the University of Western Ontario, Canada, in 2005. In 2006, he was a post-doctoral researcher at Canadian Surgical Technologies and Advanced Robotics (CSTAR), Canada. In 2007-2008, he was an NSERC Post-Doctoral Fellow at Harvard University, USA. Dr. Tavakoli's research interests broadly involve the areas of robotics and systems control. Specifically, his research focuses on haptics and teleoperation control, medical robotics, and image-guided surgery. Dr. Tavakoli is the lead author of Haptics for Teleoperated Surgical Robotic Systems (World Scientific, 2008). He is a Senior Member of IEEE and an Associate Editor for IEEE/ASME Transactions on Mechatronics, Journal of Medical Robotics Research, Control Engineering Practice, and Mechatronics.